

Validation study of the SeaWiFS oxygen A-band absorption correction: comparing the retrieved cloud optical thicknesses from SeaWiFS measurements

Menghua Wang

Validation study of the SeaWiFS oxygen A-band absorption correction: comparing the retrieved cloud optical thicknesses from SeaWiFS measurements

Menghua Wang

Atmospheric correction in ocean-color remote sensing corrects more than 90% of signals in the visible contributed from the atmosphere measured at satellite altitude. The Sea-viewing Wide Field-of-view Sensor (SeaWiFS) atmospheric correction uses radiances measured at two near-infrared wavelengths centered at 765 and 865 nm to estimate the atmospheric contribution and extrapolate it into the visible range. However, the SeaWiFS 765-nm band, which covers 745–785 nm, completely encompasses the oxygen A-band absorption. The 0, A-band absorption usually reduces more than 10–15% of the measured radiance at the SeaWiFS 765-nm band. Ding and Gordon [Appl. Opt. 34, 2068–2080 (1995)] proposed a numerical scheme to remove the O₂ A-band absorption effects from the atmospheric correction. This scheme has been implemented in the SeaWiFS ocean-color imagery data-processing system. I present results that demonstrate a method to validate the SeaWiFS 765-nm 0, A-band absorption correction by analyzing the sensor-measured radiances at 765 and 865 nm taken looking at the clouds over the oceans. SeaWiFS is usually not saturated with cloudy scenes because of its bilinear gain design. Because the optical and radiative properties of water clouds are nearly independent of the wavelengths ranging from 400 to 865 nm, the sensor-measured radiances above the cloud at the two near-infrared wavelengths are comparable. The retrieved cloud optical thicknesses from the SeaWiFS band 7 measurements are compared for cases with and without the 0, A-band absorption corrections and from the band 8 measurements. The results show that, for air-mass values of 2–5, the current SeaWiFS 0, A-band absorption correction works reasonably well. The validation method is potentially applicable for in-orbit relative calibration for SeaWiFS and other satellite sensors.

OCIS codes: 010.1290, 010.4450, 030.5620, 280.0280.

1. Introduction

The atmospheric correction of the Sea-Viewing Wide Field-of-View Sensor¹ (SeaWiFS) uses two near-infrared (NIR) bands (765 and 865 nm), where the ocean can usually be considered as a black surface, to estimate the atmospheric effect and extrapolate it into the visible.^{2,3} The Gordon-Wang atmospheric-correction algorithm assumes that, when both the ozone and the water-vapor absorptions are removed, the ocean-atmosphere system is composed of air molecules (Rayleigh scattering) and aerosols bounded by a Fresnel-reflecting ocean surface. However, the SeaWiFS 765-nm band, which covers 745–785 nm, completely encompasses the oxygen A-band absorp-

tion. The 0, A-band absorption reduces more than 10–15% of the SeaWiFS measured radiance at 765 nm. It is therefore crucial to remove the O₂ A-band absorption effects accurately at SeaWiFS band 7 before the Gordon-Wang algorithm can be applied to the SeaWiFS imagery. Accuracy in correcting the 0, absorption effects at SeaWiFS band 7 directly affects the accuracy of the retrieved ocean optical and biological products.

Ding and Gordon⁴ proposed a numerical scheme, which has been implemented in the SeaWiFS imagery data process, to remove the 0, A-band absorption effects on the SeaWiFS atmospheric correction. In this paper I present results that demonstrate a validation study for SeaWiFS band 7 O₂ A-band absorption correction by analyzing the sensor-measured radiances at the two NIR bands looking at the cloudy scenes. First I briefly review the proposed 0, A-band absorption correction and its implementation into the SeaWiFS imagery data processing system. Next I describe the SeaWiFS bilinear gain design in

The author is with the University of Maryland Baltimore County, NASA Goddard Space Flight Center, Code 970.2, Greenbelt, Maryland 20771.

Received 14 July 1998; revised manuscript received 22 October 1998.

which SeaWiFS is usually not saturated with the cloudy scenes and discuss cloud optical thickness retrieval with the SeaWiFS measurements. Finally, I demonstrate a validation scheme by comparing the cloud optical thickness retrieved from the SeaWiFS 765-nm radiance for cases both with and without the 0, A-band absorption corrections and from 865-nm measurements. The O₂ A-band absorption correction values that are derived from the SeaWiFS cloudy scenes are then compared with the Ding-Gordon results that are used in the SeaWiFS atmospheric corrections.

2. Proposed 0, A-band Absorption-Correction Scheme

Let us define the reflectance $\rho = \pi L / \mu_0 F_0$, where L is the radiance in the given viewing direction, F_0 is the extraterrestrial solar irradiance, and μ_0 is the cosine of the solar zenith angle. The total reflectance measured at the top of the ocean-atmosphere system can be written as

$$\rho_t(\lambda) = \rho_r(\lambda) + \rho_a(\lambda) + \rho_{ra}(\lambda) + t(\lambda)\rho_{wc}(\lambda) + t(\lambda)\rho_w(\lambda), \quad (1)$$

where $\rho_r(A)$ is the reflectance that results from multiple scattering by air molecules (Rayleigh scattering) in the absence of aerosols; $\rho_a(A)$ is the reflectance that results from multiple scattering by aerosols in the absence of air; $\rho_{ra}(A)$ is a multiple interaction term between molecules and aerosols; $\rho_{wc}(A)$ is the reflectance at the sea surface that arises from sunlight and skylight reflecting from whitecaps on the surface; and $\rho_w(A)$ is the water-leaving reflectance, which is a desired quantity in ocean-color remote sensing. $t(A)$ is the atmospheric diffuse transmittance⁵ that accounts for the effects of propagating water-leaving and whitecap reflectances from the sea surface to the top of the atmosphere. In Eq. (1) the surface Sun glitter term has been ignored because it has to be avoided in the atmospheric correction. The influence of whitecaps on the imagery can be estimated from an estimation of the surface wind speed.⁶ The goal of the atmospheric correction is to retrieve the water-leaving reflectance $\rho_w(A)$ accurately from spectral and angular measurements of reflectance $\rho_t(A)$ at the satellite altitude. For SeaWiFS's two NIR channels, because $\rho_{ra}(A)$ is usually negligible, Eq. (1) can be rewritten as

$$\rho_t(\lambda) - \rho_r(\lambda) - t(\lambda)\rho_{wc}(\lambda) = \rho_a(\lambda) + \rho_{ra}(\lambda). \quad (2)$$

Therefore the effects of aerosols and Rayleigh-aerosol interactions $\rho_a(A) + \rho_{ra}(A)$ on the imagery can be estimated at the two NIR bands from sensor-measured radiances, the computed Rayleigh scattering reflectances, and the estimated whitecap contributions. This quantity is then extrapolated and removed in the visible. Obviously, to correct the atmospheric effects in the visible accurately it is important first to estimate accurately the effects of $\rho_r(A) + \rho_{ra}(A)$ at the two NIR bands.

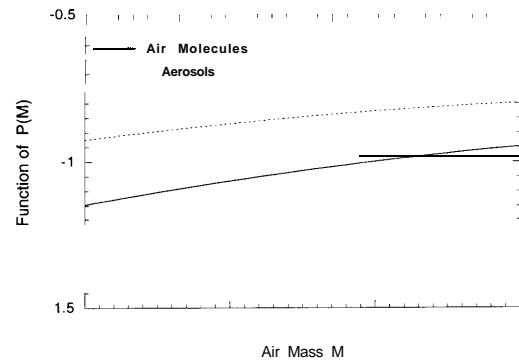


Fig. 1. SeaWiFS 0, A-band absorption correction function $P(M)$ as a function of air mass M for air molecules and aerosols. Redrawn from the results of Ding and Gordon.⁴

In studies of the effects of O₂ A-band absorption on atmospheric correction of ocean-color imagery, Ding and Gordon⁴ and Fraser⁷ found that the O₂ A-band absorption affects more than 10–15% of SeaWiFS band 7; i.e., the sensor-measured radiance at SeaWiFS band 7 was reduced by more than 10–15% because of the absorption. Following the Ding-Gordon notations, we define, at SeaWiFS band 7, the reflectances of aerosols and the Rayleigh-aerosol interactions as

$$\rho_A'(\lambda) = \rho_a'(\lambda) + \rho_{ra}'(\lambda), \quad \rho_A(\lambda) = \rho_a(\lambda) + \rho_{ra}(\lambda), \quad (3)$$

where ρ_A' and ρ_A are, respectively, reflectance with and without the 0, A-band absorption present. Because implementation of the SeaWiFS atmospheric correction was achieved through the use of lookup tables for $\rho_r(A) + \rho_a(A)$ for different aerosol optical properties (12 aerosol models with various optical thicknesses) and various solar and viewing geometries at the SeaWiFS 8 spectral bands, correction of the 0, A-band absorption at SeaWiFS band 7 is in effect an effort to find a relationship between ρ_A and ρ_A' , i.e., to recover the value of ρ_A from ρ_A' . Through a series of radiative transfer simulations, Ding and Gordon developed a numerical method to correct the O₂ A-band absorption. First, because Rayleigh scattering is well understood, the relationship between ρ_r and ρ_r' was obtained as a numerical fitting, in which ρ_r' was related to ρ_r through a power function of air mass M , defined as $M = 1/\cos \theta_0 + 1/\cos \theta$, where θ_0 and θ are, respectively, the solar and sensor zenith angles. Next, ρ_A' was computed from sensor-measured ρ_t' and ρ_r' estimated from Eqs. (3). Finally, by use of a realistic aerosol profile, ρ_A was related to ρ_A' by numerical fitting. Ding and Gordon⁴ found that both ρ_r and ρ_A can be related to ρ_r' and ρ_A' as a function of M as

$$\rho_{r,A} = [1 + 10^{P_{r,A}(M)}] \rho_{r,A}', \quad (4)$$

where $P_{r,A}(M)$ is a fitting function of air mass M for the Rayleigh (r) and aerosol (A) components. Figure 1 shows the redrawn O₂-correction function $P_{r,A}(M)$ from Ding and Gordon as a function of air mass M from 2 to 5 for both the Rayleigh and the aerosol components. Through the simulations Ding and

Gordon concluded that for the Rayleigh scattering component Eq. (4) is accurate to within $\sim 0.2\%$, whereas for the ρ_A term, although the accuracy of Eq. (4) depends on the aerosol model profile, the error is usually within 1–2% for $M \leq 5$. Inasmuch as the Rayleigh scattering is well known and can be predicted accurately, validation of the oxygen A-band absorption correction at SeaWiFS band 7 in effect validates the accuracy of Eq. (4) for the relationship between ρ_A and ρ_A' . Note that the correction function $P_{r,A}(M)$ is a function only of air mass (M) and is independent of the concentration of either air molecules or aerosols. Therefore the function $P_A(M)$ is applicable to a water cloud composed of particles of water droplets.

The implementation of the band 7 0, A-band absorption correction in the SeaWiFS data-processing system is straightforward. With both precalculated functions of $P_r(M)$ and $P_A(M)$ for various M values, the SeaWiFS band 7 $p_{r,A} + p_{r,A}$ value can be computed from Eqs. (3) and (4). Both bands 7 and 8 $p_{r,A} + p_{r,A}$ values can then be used to correct the atmospheric effects in the visible by use of the Gordon-Wang atmospheric correction algorithm.

3. Validation Study of Eq. (4) from SeaWiFS Cloudy Scenes

In this section I first briefly describe the SeaWiFS bilinear gain design in which SeaWiFS is usually not saturated for cloudy scenes while it retains its high sensitivity for the ocean color measurements. Then the cloud optical thickness retrievals by use of the SeaWiFS measurements is discussed, and a comparison is made of results for retrieved cloud optical thickness from the SeaWiFS bands 7 and 8 measurements in validating the SeaWiFS O_2 A-band absorption correction. Finally, the O_2 A-band absorption correction factors are derived by comparison of the SeaWiFS bands 7 and 8 measurements made toward the cloudy scenes.

A. SeaWiFS Bilinear Gain Design

The SeaWiFS was designed as a bilinear gain instrument for the large dynamic response range so it could measure cloud radiance. The initial reason for adopting the bilinear gain design was that with it the instrument could perform a postlaunch correction for the sensor stray-light contamination by the clouds.⁸ Figure 2 shows the relationship between radiance and digital counts of the sensor response function for SeaWiFS spectral bands 2 (443 nm), 6 (670 nm), 7 (765 nm), and 8 (865 nm). The SeaWiFS's other spectral bands have similar response functions. SeaWiFS uses 10 bits digitized for the eight spectral channels, and each channel's output ranges from 0 to 1023 counts. As shown in Fig. 2, whereas the SeaWiFS maintains very high sensitivity at low radiance levels (approximately the first 800 counts) for the ocean-color measurements, it is usually not saturated for the cloudy scenes because of its low sensitivity to the high radiance level.

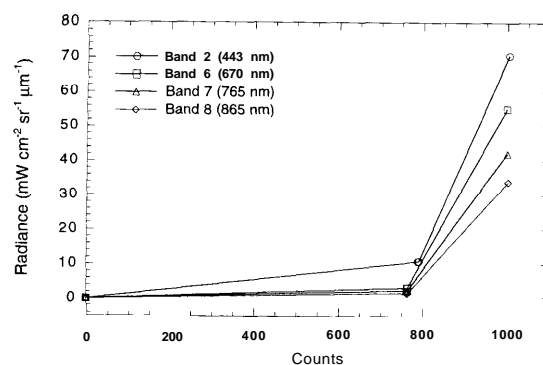


Fig. 2. SeaWiFS bilinear gain response function for SeaWiFS channels 443, 670, 765, and 865 nm.

B. Relationship between Cloud Top Reflectance and Cloud Optical Thickness

In the remote retrieval of cloud microphysical, optical, and radiative properties from aircraft or satellite sensors the sensor-measured radiance at wavelengths ranging from 400 to 865 nm is primarily a function of cloud optical thickness, whereas the long NIR radiances (e.g., 1.6, 2.1, and 3.7 μm) are sensitive both to optical thickness and, especially, to cloud water-droplet size.^{9–11} The sensor-measured radiance at the visible band can therefore be used to refer to the cloud optical thickness, whereas the long NIR radiances can be used to retrieve the cloud water-droplet size. The scattering of cloud water droplets has a Mie scattering character, and its optical properties are nearly independent of the visible wavelength. At wavelengths ranging from 400 to 865 nm the cloud water droplet is nearly nonabsorbing (pure scattering), and its scattering phase function is characteristically strongly peaked in the forward direction. Figure 3 illustrates the water cloud scattering phase functions for SeaWiFS wavelengths 412, 670, and 865 nm with an effective particle radius of 8 μm . Figure 3 shows that the water cloud scattering phase functions are similar for wavelengths ranging from 412 to 865 nm.

To understand the relationship between the mea-

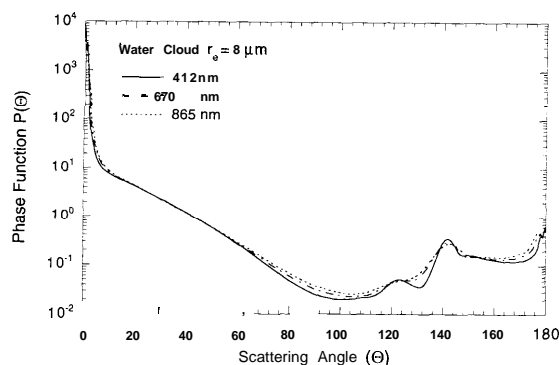


Fig. 3. Water cloud scattering phase function as a function of scattering angle at SeaWiFS wavelengths 412, 670, and 865 nm. The water cloud is assumed to have an effective particle radius of 8 μm .

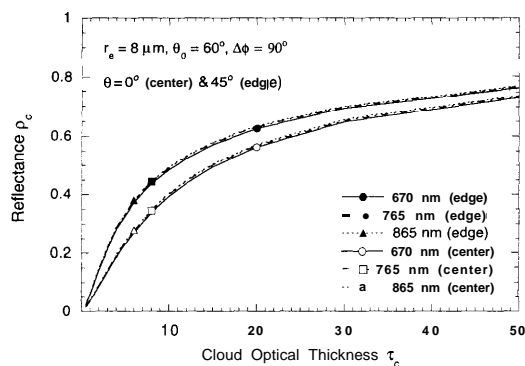


Fig. 4. Cloud top reflectance as a function of cloud optical thickness for SeaWiFS wavelengths 670, 765, and 865 nm for a solar zenith angle of 60° , viewing angles of 0° (center) and 45° (edge), and relative azimuthal angle of 90° .

sured cloud top reflectance and the cloud optical thickness at the various SeaWiFS spectral bands, I carried out simulations for a one-layer water cloud overlying a flat ocean surface for various cloud optical thicknesses and different solar and viewing geometries. Figure 4 provides an example of results for measured reflectance as a function of cloud optical thickness for SeaWiFS wavelengths of 670, 765, and 865 nm, solar zenith angle of $\theta_0 = 60^\circ$, viewing angles of 0° (center) and 45° (edge), and relative azimuthal angle of $\Delta\phi = 90^\circ$. Note that, in computing the cloud top reflectance for SeaWiFS band 7, it was assumed that the O_2 A-band absorption was not present. It is obvious from Fig. 4 that, for a given cloud optical thickness and solar and viewing geometry, the measured reflectance at the cloud top is nearly independent of the wavelength; i.e., the cloud top reflectance is almost identical for SeaWiFS bands 6–8. Therefore one would expect that, if there were no O_2 A-band absorption at SeaWiFS band 7, the retrieved cloud optical thickness from measurements of SeaWiFS bands 7 and 8 would be comparable. By comparing the retrieved cloud optical thickness from the SeaWiFS measurements at band 7 with the 0, A-band absorption removed and the band 8 measurements, one can study the efficacy of the SeaWiFS band 7 0, A-band absorption-correction algorithm.

C. Cloud Optical Thickness Retrieval from SeaWiFS Bands 7 and 8 Measurements

I implemented a cloud optical thickness retrieval algorithm of Nakajima and King,¹¹ using the SeaWiFS measured radiances at bands 7 and 8. This cloud retrieval algorithm was used in studying the Rayleigh scattering effects in cloud optical thickness retrievals.¹² Briefly, the relationship between cloud top reflectance and cloud optical thickness as in Fig. 4 was first generated as lookup tables for a fixed effective water droplet size ($r_e = 8 \mu\text{m}$), various cloud optical thicknesses τ_c , different solar and viewing geometries, and at SeaWiFS spectral bands 7 (765 nm) and 8 (865 nm). After correction of the Rayleigh scattering effects, the SeaWiFS measured radiances

Table 1. Comparison of Four Cases of Acquired SeaWiFS Cloudy Imagery

Case	Date Acquired (1997)	Data Size (Pixel \times Scan)	Location (Longitude, Latitude)
(a)	4 September	1285 \times 2200	$-60^\circ, 36''$
(b)	26 September	1285 \times 440	$165^\circ, -52''$
(c)	3 October	1285 \times 360	$195^\circ, 23''$
(d)	11 October	1285 \times 3420	$-54^\circ, 40''$

at bands 7 and 8 can then be converted into cloud optical thickness through comparisons with the pre-calculated lookup radiance library. As discussed by Wang and King,¹² the Rayleigh scattering effects in the cloud optical thickness retrievals at SeaWiFS band 8 is usually negligible, whereas at band 7 it is usually small. Therefore the Rayleigh scattering effects on SeaWiFS band 7 can be removed by use of the single-scattering approximation.

To assess effects of the O_2 A-band absorption in the SeaWiFS band 7, we can compute the cloud optical thickness from the SeaWiFS band 7 measurements in two ways: with and without 0, A-band absorption removed at the band 7. For a cloudy scene we can rewrite Eqs. (3) for SeaWiFS band 7 as

$$\rho_c'(\lambda) = \rho_t'(\lambda) - \rho_r'(\lambda), \quad \rho_c(\lambda) = \rho_t(\lambda) - \rho_r(\lambda), \quad (5)$$

where ρ_c' and ρ_c are, respectively, cloud top reflectance with and without the 0, A-band absorption present for SeaWiFS wavelength 765 nm. The reflectance values of ρ_c' and ρ_c are then converted into cloud optical thicknesses $\tau_c'(\lambda)$ and $\tau_c(\lambda)$, respectively, through comparisons with the lookup tables. On the other hand, the SeaWiFS measured radiance at band 8 can be converted into cloud optical thickness $\tau_c(865)$ by the Nakajima-King cloud retrieval algorithm.¹¹ Note that by using Eqs. (5) in deriving the cloud optical thickness from the SeaWiFS measurements we implicitly assume that the effects of radiance contributed by scattering the Rayleigh-cloud interactions on the retrieved cloud optical thickness are negligible for SeaWiFS band 7.

SeaWiFS cloud optical thickness retrievals were performed for four images acquired during a period in September and October of 1997 at various locations over the ocean. Table 1 lists acquired dates, locations, and data sizes for these four images. Figure 5 shows SeaWiFS band 8 radiance images obtained on 4 and 8 September and 3 and 11 October 1997. The figure includes scans of 2200, 440, 360, and 3420, respectively, with 1285 pixels for each scan. Note that for all the results presented in this paper the SeaWiFS preflight calibration coefficients were used in generating the SeaWiFS measured radiances. Cloud optical thickness was retrieved by use of the SeaWiFS band 7 measurements both with and without the O_2 A-band absorption corrections and from the band 8 measurements. Figure 6 shows the probability-distribution function (PDF; %) of the retrieved cloud optical thickness for various retrievals

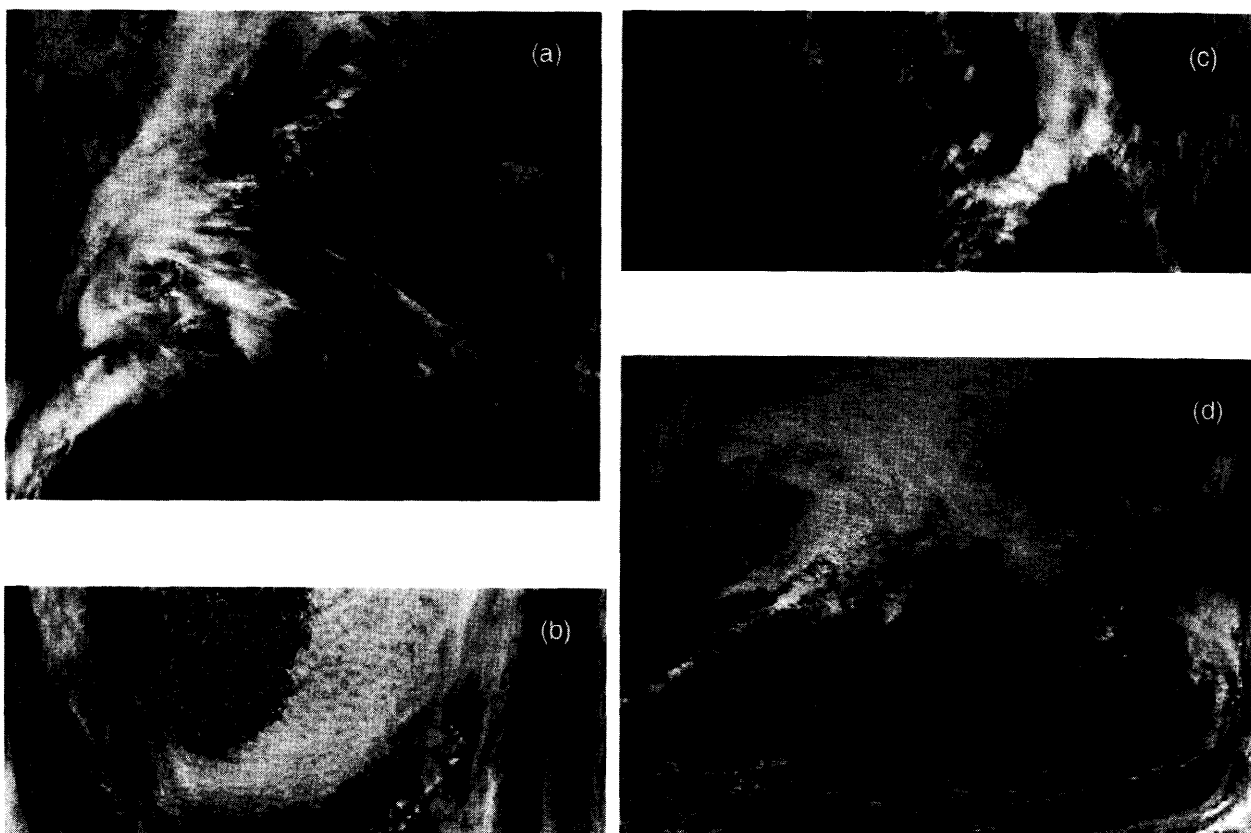


Fig. 5. SeaWiFS band 8 (865-nm) radiance images acquired in 1997 on (a) 4 September, (b) 26 September, (c) 3 October, and (d) 11 October.

obtained by use of the SeaWiFS measurements shown in Fig. 5. Figures 6(a), 6(b), 6(c), and 6(d) include total retrieved cloud optical thickness data of 2.1×10^5 , 6.9×10^4 , 3.3×10^4 , and 3.0×10^5 , respectively, for each curve. In generating the PDF curves in Fig. 6 I used data for which the retrieved cloud optical thickness was $2 \leq \tau_c(865) \leq 6$, i.e., the thin water clouds for reasons of high sensitivity to τ_c variations and for confined low-level water clouds corresponding to a similar profile used by Ding and Gordon.⁴ The SeaWiFS retrieved cloud optical thicknesses at the blue were compared with the 865-nm band to identify the low-level water clouds. In this comparison, the larger the difference between the blue and the 865-nm bands, the larger the Rayleigh scattering contributions were above the clouds and the lower the cloud level. Figure 6 shows that the shapes of the PDF's are similar for all three retrievals. However, there is clear evidence indicating that the O_2 A-band absorption at 765 nm leads to underestimates of the cloud optical thickness, as expected. Results at both 765 nm with the O_2 A-band absorption correction and at 865 nm for all four cases are really identical, indicating that the O_2 A-band absorption-correction algorithm worked quite well, whereas the retrievals at 765 nm without the O_2 A-band absorption corrections shifted toward the smaller values of the cloud optical thickness.

To evaluate the accuracy of the O_2 A-band absorp-

tion correction, we calculate the difference of the retrieved cloud optical thicknesses between band 7 with and without the O_2 A-band absorption corrections and the band 8 results. We define

$$\Delta\tau_c'(765) = \tau_c'(765) - \tau_c(865),$$

$$\Delta\tau_c(765) = \tau_c(765) - \tau_c(865)$$

as the difference in retrieved cloud optical thicknesses between SeaWiFS band 7 with and without the O_2 A-band absorption corrections and the band 8 measurements. Figure 7 gives the PDF's of both $\Delta\tau_c'(765)$ (%) and $\Delta\tau_c(765)$ (%) computations for the four cases of the thin clouds [$2 \leq \tau_c(865) \leq 6$] shown in Figs. 5 and 6. The solid curves and the dashed curves are, respectively, the PDF (%) for $\Delta\tau_c'(765)$ (%) and $\Delta\tau_c(765)$ (%) computations. Figure 7 shows that, without the O_2 A-band absorption correction, the retrieved cloud optical thickness at band 7 $\tau_c'(765)$ is underestimated by approximately 10–15% in most cases. When the O_2 A-band absorption corrections are used, the difference between $\tau_c(765)$ and $\tau_c(865)$ is reduced to approximately 0–3% in most cases. The peaks of the PDF's of the differences for all four cases were moved from $\Delta\tau_c'(765)$ of approximately -10 to -15% to $\Delta\tau_c(765)$ of -0%. It is obvious by a comparison of the band 8 and band 7 results that the accuracy of the retrieved cloud optical thickness at SeaWiFS band 7 improves significantly by

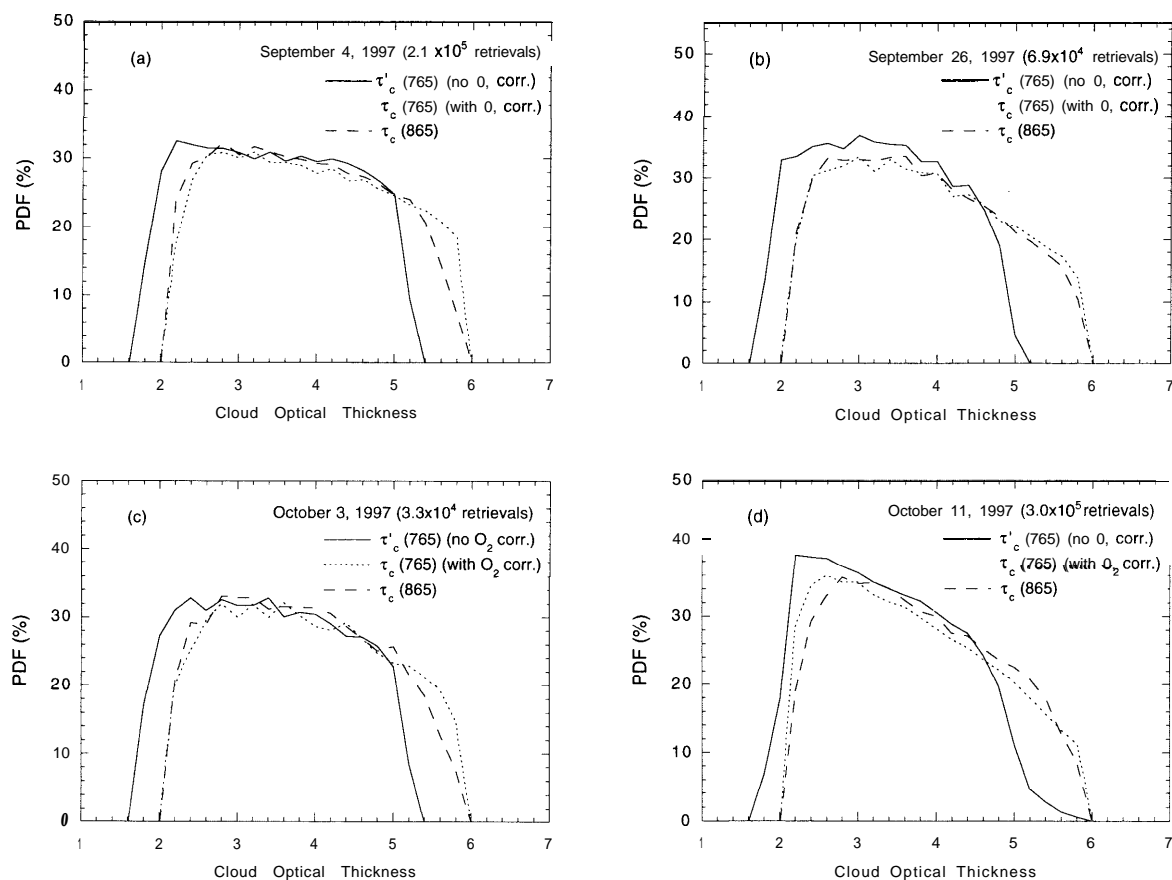


Fig. 6. PDF (%) of the retrieved cloud optical thickness for $2 \leq \tau_c(865) \leq 6$ from the SeaWiFS measurements corresponding to cloudy scenes obtained on the dates shown. There are three retrievals: SeaWiFS band 7 with and without the 0, A-band absorption corrections and from band 8 measurements.

addition of the SeaWiFS 0, A-band absorption corrections.

D. Derivation of the Relationship between ρ_c and ρ'_c from SeaWiFS Measurements

By assuming that the retrieved cloud optical thickness is independent of the SeaWiFS wavelengths at 765 and 865 nm, we can derive the relationship between ρ_c and ρ'_c for SeaWiFS band 7 from the bands 7 and 8 measurements. Figure 8 provides the derived $P_A(M)$ values from the four cases of the SeaWiFS cloudy scenes presented in Figs. 5 and 6 compared with the Ding-Gordon results. In generating Fig. 8 I obtained each point of the $P_A(M)$ value, with the corresponding M value from the SeaWiFS cloudy scenes, by averaging over all possible values from the four cases in Figs. 5 and 6 for cloud optical thicknesses $2 \leq \tau_c(865) \leq 6$. The error bar at each point is the variation of $\pm\sigma$ values from computations. The solid curve is a least-squares quadratic fit to the derived $P_A(M)$ values. Also, the number of data points used in the average computations for each point is plotted in the same figure. For example, for $M = 2.1$ the derived $P_A(M)$ value from averaging over the four SeaWiFS cloud scenes is -0.914 (-0.920 from Ding and Gordon) with variations of σ

$= \pm 0.130$ and a total of -4.1×10^3 retrievals in this computation. For $M = 5.0$ the derived average $P_A(M)$ value is -0.776 (-0.798 from Ding and Gordon) with variations of $\sigma = 20.065$ and a total of -3.7×10^3 data in the computation. However, because $P_A(M)$ is expected to be a smooth function of air mass M , the least-squares quadratic fitting derived from these average data is more reasonable. Table 2 lists the values of fitting coefficients for $P_A(M)$ that were derived from the cloudy scenes and compares them with the values derived by Ding and Gordon.

To evaluate the accuracy of the $P_A(M)$ and corrected ρ_A values quantitatively we compute the differences (%) between the derived and the current SeaWiFS $P_A(M)$ values and the ρ_A values obtained by use of the corresponding $P_A(M)$ functions for the band 7 O₂ A-band absorption correction. Figure 9 provides these computations. In computing the difference (%) between derived and SeaWiFS $P_A(M)$ values I used the derived least-squares fit values (solid curve in Fig. 8); i.e., the difference between the solid and the dotted curves in Fig. 8. Figure 9 shows that, for air-mass values of 2-5, the difference in $P_A(M)$ is usually within $\sim 3\%$, whereas the difference in ρ_A is within 1%. Figures 8 and 9 show that, for air-mass values of 2-5, the derived 0, A-band absorption-

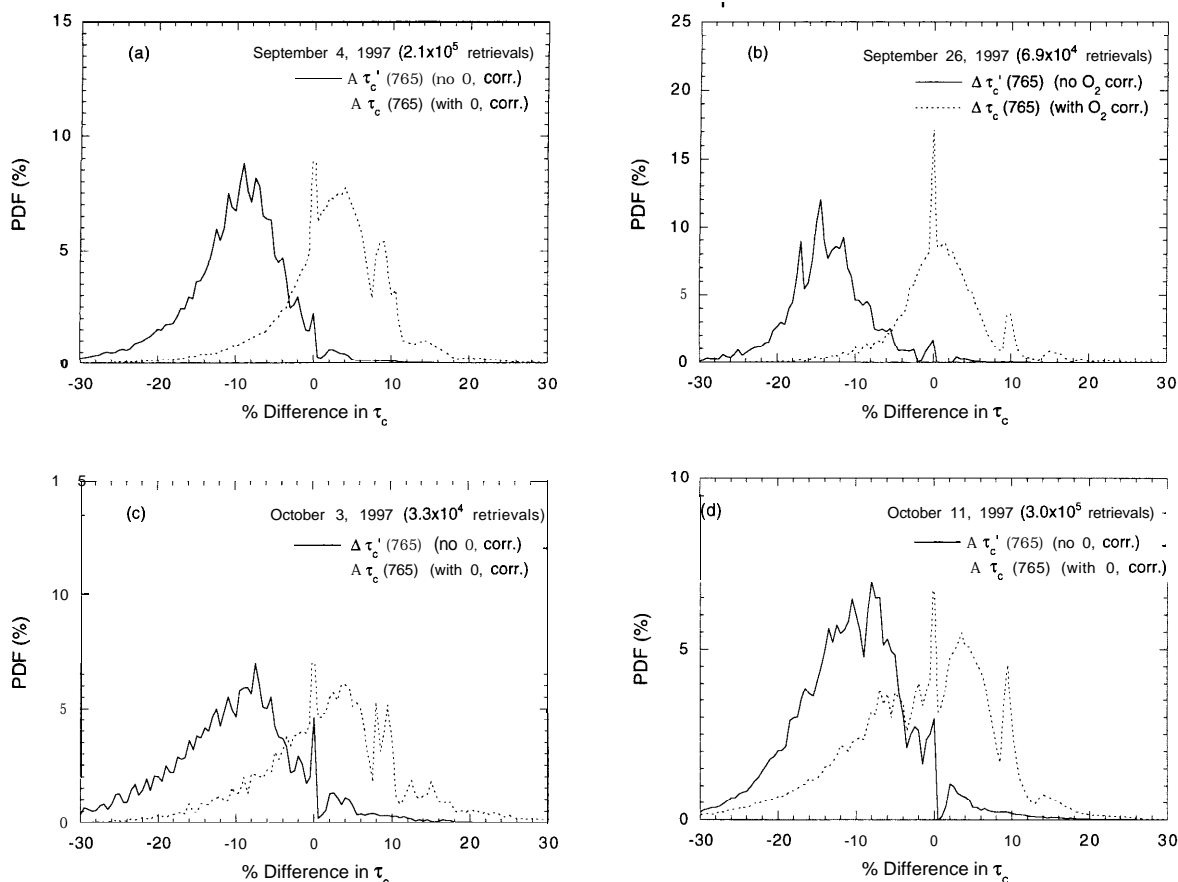


Fig. 7. PDF (%) of the differences $\Delta\tau_c'(765)$ and $\Delta\tau_c(765)$ (%) in retrieved cloud optical thickness for $2 \leq \tau_c(865) \leq 6$ from the SeaWiFS measurements corresponding to cloudy scenes measured on the dates listed.

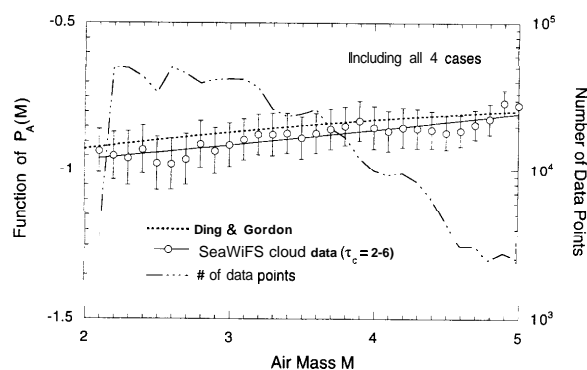


Fig. 8. Derived values of $P_A(M)$ from the four cases of SeaWiFS cloudy scenes compared with values of Ding and Gordon. The error bar corresponding to each point is the variation of $\pm\sigma$ values from the computation, and the solid curve is a least-squares quadratic fit to the points. The curve for the number of data contributed to the average computations in the derivation of $P_A(M)$ by the four cases of cloudy scenes is keyed to the right-hand y axis.

correction factors from the SeaWiFS cloudy scenes agree quite well with the Ding-Gordon values. It is therefore concluded from these studies that the current SeaWiFS oxygen A-band absorption correction algorithm for the wavelength 765 nm works reasonably accurately.

Table 2. Fitting Coefficients for $P_A(M) = a_0 + a_1M + a_2M^2$ Derived from Cloudy Scenes Compared with Values from Ding and Gordon

Coefficient	Derived from Cloudy Scenes	Ding-Gordon Value ^a
a_0	-1.0531	-1.0796
a_1	0.0536	0.0905
a_2	-0.0005	-0.0068

^aRef. 4.

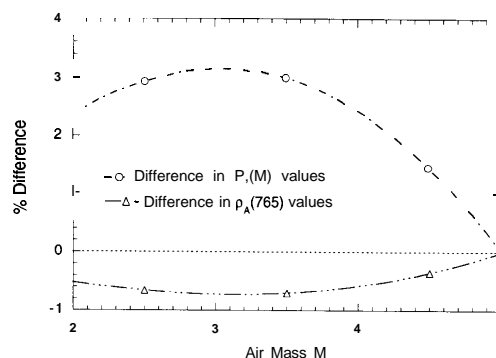


Fig. 9. Differences (%) between the values derived from cloudy scenes and the current SeaWiFS $P_A(M)$ and ρ_A values for the SeaWiFS band 7 O₂ A-band absorption corrections.

4. Conclusions

Based on the fact that the water cloud optical properties are nearly independent of wavelengths that range from 400 to 865 nm, we have evaluated the accuracy of the SeaWiFS oxygen A-band absorption corrections algorithm by comparing the retrieved cloud optical thicknesses from the SeaWiFS band 7 measurements both with and without the oxygen A-band absorption corrections and from the band 8 measurements. The results show that, with the O₂ A-band absorption corrections, the difference in the retrieved cloud optical thickness between the SeaWiFS band 7 and band 8 measurements was reduced from a negative value of approximately 10–15% to approximately 0–3% in most cases. For air-mass values ranging from 2 to 5, the derived 0, A-band absorption correction function $P_A(M)$ agreed well with the values proposed by Ding and Gordon. The difference between the derived values from the SeaWiFS cloudy scenes and the current SeaWiFS 0, A-band absorption correction function is usually within ~3%, which leads to a difference in ρ_A within 1% for air-mass values ranging from 2 to 5.

Because the cloud optical properties, in particular, the water cloud optical depth, are nearly independent of the SeaWiFS wavelengths from 412 to 865 nm it is possible to monitor the temporal variation of the sensor performance for the eight SeaWiFS spectral channels by comparing sensor-measured radiance over cloudy scenes within the bands. This technique for monitoring sensor performance, however, is relative; i.e., it does not provide any information regarding the absolute accuracy of the SeaWiFS channels. The validation method is also potentially applicable for in-orbit relative calibration for SeaWiFS and other satellite sensors.

This research was supported by funding provided by the National Aeronautics and Space Administration under the Sensor Intercomparison and Merger for Biological and Interdisciplinary Oceanic Studies (SIMBIOS) project.

References

1. S. B. Hooker, W. E. Esaias, G. C. Feldman, W. W. Gregg and C. R. McClain, *An Overview Of SeaWiFS and Ocean Color*, Vol. 1 of SeaWiFS Tech. Rep. Series, NASA Tech. Memo. 104566 (NASA Goddard Space Flight Center, Greenbelt, Md., 1992).
2. H. R. Gordon and M. Wang, "Retrieval of water-leaving radiance and aerosol optical thickness over the oceans with SeaWiFS: a preliminary algorithm," *Appl. Opt.* **33**, 443-452 (1994).
3. H. R. Gordon, "Atmospheric correction of ocean color imagery in the Earth Observing System era," *J. Geophys. Res.* **102**, 17,081-17,106 (1997).
4. K. Ding and H. R. Gordon, "Analysis of the influence of 0, A-band absorption on atmospheric correction of ocean color imagery," *Appl. Opt.* **34**, 2068-2080 (1995).
5. H. Yang and H. R. Gordon, "Remote sensing of ocean color: assessment of water-leaving radiance bidirectional effects on atmospheric diffuse transmittance," *Appl. Opt.* **36**, 7887-7897 (1997).
6. H. R. Gordon and M. Wang, "Influence of oceanic whitecaps on atmospheric correction of ocean-color sensor," *Appl. Opt.* **33**, 7754-7763 (1994).
7. R. S. Fraser, *The Effect Of Oxygen Absorption on Band-7 Radiance*, Vol. 27 of SeaWiFS Tech. Rep. Series, NASA Tech. Memo. 104566 (NASA Goddard Space Flight Center, Greenbelt, Md., 1995).
8. R. A. Barnes, A. W. Holmes, and W. E. Esaias, *Stray Light in the SeaWiFS Radiometer*, Vol. 31 of SeaWiFS Tech. Rep. Series, NASA Tech. Memo. 104566 (NASA Goddard Space Flight Center, Greenbelt, Md., 1995).
9. S. Twomey and T. Cocks, "Spectral reflectance of clouds in the near-infrared: comparison of measurements and calculations," *J. Meteorol. Soc. Jpn.* **60**, 583-592 (1982).
10. S. Twomey and T. Cocks, "Remote sensing of cloud parameters from spectral reflectance measurements in the near-infrared," *Beitr. Phys. Atmos.* **62**, 172-179 (1989).
11. T. Nakajima and M. D. King, "Determination of the optical thickness and effective particle radius of clouds from reflected solar radiation measurements. I. Theory," *J. Atmos. Sci.* **47**, 1878-1893 (1990).
12. M. Wang and M. D. King, "Correction of Rayleigh scattering effects in cloud optical thickness retrievals," *J. Geophys. Res.* **102**, 25,915-25,926 (1997).